IgG hexamers initiate acute lung injury

Simon J. Cleary[1], Yurim Seo[1], Jennifer J. Tian[1], Nicholas Kwaan[1], David P. Bulkley[2], Arthur E. H. Bentlage[3], Gestur Vidarsson[3], Éric Boilard[4], Rolf Spirig[5], James C. Zimring[6], Mark R. Looney[1]*

[1]Department of Medicine, University of California, San Francisco (UCSF), CA, USA.

[2]Department of Biochemistry and Biophysics, University of California, San Francisco (UCSF), CA, USA.

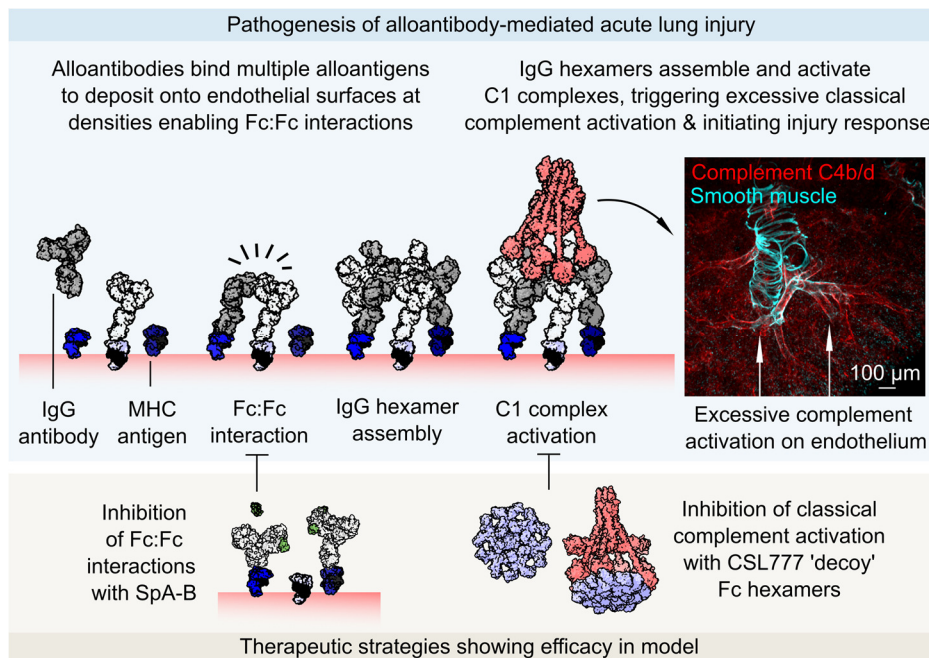[3]Sanquin Research, Amsterdam, The Netherlands.

[4]Centre de Recherche du Centre Hospitalier Universitaire de Québec - Université Laval, Québec, QC, Canada.

[5]CSL Behring, Research, CSL Behring Biologics Research Center, Bern, Switzerland.

[6]Department of Pathology, University of Virginia School of Medicine, Charlottesville, VA, USA.

*Correspondence to: mark.looney@ucsf.edu

Graphical abstract

1   Abstract

2   Antibodies can initiate lung injury in a variety of disease states such as autoimmunity, transfusion

3   reactions, or after organ transplantation, but the key factors determining in vivo pathogenicity of injury-

4   inducing antibodies are unclear. A previously overlooked step in complement activation by IgG

5   antibodies has been elucidated involving interactions between IgG Fc domains that enable assembly of

6   IgG hexamers, which can optimally activate the complement cascade. Here, we tested the in vivo

7   relevance of IgG hexamers in a complement-dependent alloantibody model of acute lung injury. We

8   used three approaches to block alloantibody hexamerization (antibody carbamylation, the K439E Fc

9   mutation, or treatment with domain B from Staphylococcal protein A), all of which reduced acute lung

10   injury. Conversely, Fc mutations promoting spontaneous hexamerization made a harmful alloantibody

11   into a more potent inducer of acute lung injury and rendered an innocuous alloantibody pathogenic.

12   Treatment with a recombinant Fc hexamer 'decoy' therapeutic protected mice from lung injury,

13   including in a model with transgenic human FCGR2A expression that exacerbated pathology. These

14   results indicate a direct in vivo role of IgG hexamerization in initiating acute lung injury and the potential

15   for therapeutics that inhibit or mimic hexamerization to treat antibody-mediated diseases.

16

17   Brief summary

18   IgG antibodies can form hexamers. This study shows that hexamer assembly is an important event

19   determining the ability of IgG to trigger acute lung injury.

Introduction

Antibodies and the complement cascade mediate protective immunity but can both become misdirected to cause harm in autoimmune and alloimmune diseases. Some antibodies can direct activation of the complement cascade at their targets, an event associated with severe pathology in disease states including several forms of transfusion reactions (1, 2), immune rejection after solid organ transplantation (3), and complications of pregnancy (4). Complement-activating alloantibodies are known mediators of transfusion-related acute lung injury (TRALI) (5, 6), a leading cause of transfusion-related deaths (7), and are linked to particularly poor outcomes following solid organ transplantation (3, 8). Complement activation by autoreactive antibodies also contributes to pathogenesis of forms of autoimmune hemolytic anemia (9), small vessel vasculitis (10), and neurological autoimmune disease (11).

Immunoglobulin G (IgG) antibodies are the most prevalent type of antibody in circulation and complement-activating alloantibodies are frequently IgG class. IgG antibodies achieve complement activation through recruiting and activating C1 complexes, each of which contain six Fc-binding domains (12, 13). A theory for how IgG achieves C1 complex activation involves groups of six IgG antibodies interacting through their Fc domains to form IgG hexamers (14). This theory recently gained experimental support from direct imaging of IgG1 and IgG3 hexamer assembly on antigenic liposomes (15, 16), with in vitro studies connecting IgG hexamerization to increased complement deposition on target surfaces (15, 17, 18). However, it is currently unclear whether IgG hexamer assembly is important in vivo in the pathogenesis of complement-dependent forms of alloantibody-mediated disease.

Here, we report testing of interventions that exploit IgG hexamerization in a mouse model of acute lung injury driven by alloantibody deposition in the pulmonary microvasculature, a process that drives pathology in forms of both TRALI and antibody-mediated rejection (AbMR) of lung transplants (6). Our results identify key molecular events driving alloantibody-mediated pathophysiology in vivo. We also demonstrate preclinical efficacy of new therapeutic approaches that prevent pathology of complement-dependent organ damage caused by alloantibodies, serving as a rationale to pursue translational studies in human alloantibody driven disease.

48 **Results**

49 Alloantibodies are prevalent but not always harmful, so determining whether alloantibodies are clinically

50 significant is a frequent conundrum in transfusion and transplantation medicine. Reflecting this clinical

51 challenge, of the many mouse monoclonal alloantibodies targeting major histocompatibility complex

52 (MHC) class I antigens, only clone 34-1-2S triggers acute lung injury when microgram quantities are

53 intravenously injected into mice (19, 20). In addition, only mice expressing the H-2^d MHC class I

54 haplotype are known to be susceptible to injury caused by the 34-1-2S antibody (5, 6). Curiously, the

55 34-1-2S antibody does not readily cause injury in H-2^b mice, including the widely used C57BL/6 (B6)

56 strain, despite the fact that it binds to MHC class I antigens expressed by H-2^b mice (5, 6). We aimed to

57 measure the affinity of 34-1-2S for a range of MHC class I antigens to improve our understanding of the

58 factors determining the ability of antibodies to cause injury in both this widely used model and more

59 generally in antibody-mediated disease states.

60 We measured the binding affinity of 34-1-2S antibody to each of the classical MHC class I antigens

61 present on injury-resistant H-2^b B6 mice and injury-susceptible H-2^d mice (**Fig. 1A**). Of the three MHC

62 antigens in the H-2 locus (K, D, and L), B6 mice only express K^b and D^b, and we detected binding of

63 34-1-2S to K^b but not D^b. In contrast, we detected binding of 34-1-2S to all three MHC class I antigens

64 from H-2^d mice, with high affinity binding to K^d and D^d, and weak binding to L^d (**Fig. 1B**). Other MHC

65 class I antibodies (clones AF6-88.5.5.3, 20-8-4S, SF1.1.10, 30-5-7S and 34-5-8S), which do not readily

66 induce injury (5)) each bound to only one MHC class I antigen from each MHC type (**Fig. S1**).

67 Together, the above findings led us to the hypothesis that the ability of 34-1-2S to induce lung injury in

68 H-2^d mice is a function of increased density of bound antibody in H-2^d animals resulting from 34-1-2S

69 simultaneously binding K^d, D^d, and possibly L^d. This hypothesis was tested by injecting 34-1-2S

70 antibody into B6.ConK^d-on mice, which express K^d but do not express D^d or L^d (21). B6.*H2^d* mice

71 expressing the full complement of MHC class I antigens recognized by 34-1-2S (K^d, D^d, and L^d) were

72 used as background-matched positive controls for susceptibility to injury (**Fig. 1C**). In contrast to

73 B6.*H2^d* mice, B6.ConK^d-on mice did not develop lung injury (**Fig. 1D, E**). These data are consistent with

74 34-1-2S antibody causing injury in H2^d mice through high affinity binding to multiple MHC class I

75 antigens.

76 Engagement of multiple antigens can permit high density antibody deposition, an event associated with

77 classical complement activation. Complement activation has been implicated in pathogenesis of acute

78 lung injury caused by 34-1-2S antibody, but previous studies have not determined whether injury in this

79 model is directly triggered by antibody-mediated complement activation via the classical pathway (5, 6).

80   To test whether 34-1-2S-induced injury requires classical complement activation, we bred mice

81   expressing the $H2^d$ susceptibility locus with mice lacking C1qa (22), a protein that is necessary for

82   classical complement activation as it is one of the three proteins which make up each of the six Fc-

83   binding C1q subcomponents in each C1 complex (**Fig. 2A**).

84   Relative to B6.$H2^d$:$C1qa^{+/+}$ littermate controls, C1qa-deficient B6.$H2^d$:$C1qa^{-/-}$ mice were resistant to

85   alloantibody-mediated acute lung injury and mortality (**Fig. 2B-D**). Mice lacking C1qa were also

86   protected from deposition of complement component C3 split products on the endothelium of

87   pulmonary capillaries (**Fig. 2E**). Staining for C1qa in lungs confirmed absence of C1qa protein in

88   knockout mice, with intense C1 complex deposition seen around pulmonary arteriolar endothelial cells

89   in *C1qa*-expressing mice injected with 34-1-2S antibody (**Fig. 2F**).

90   To identify the microanatomical site of classical complement activation, we stained lungs of mice

91   injected with 34-1-2S for the complement split products C4b and C4d, which form covalent bonds with

92   proteins at sites of classical complement activation. We observed strong positivity for C4b/d highlighting

93   the endothelium of medium and small-sized pulmonary arterioles in B6.$H2^d$:$C1qa^{+/+}$ mice injected with

94   34-1-2S, but not in B6.$H2^d$:$C1qa^{-/-}$ mice (**Fig. 2G** and **Movie S1**). Together, these results indicate that

95   34-1-2S causes acute lung injury because this antibody is deposited onto the pulmonary arteriolar

96   endothelium at densities sufficient to trigger excessive classical complement activation directed at the

97   walls of these blood vessels.

98   Dense binding to membrane-expressed antigens would be expected to facilitate IgG Fc:Fc interactions

99   and IgG hexamer assembly. IgG hexamers are potent activators of C1 complexes in vitro (15), and are

100   further implicated in classical complement activation by models for C1 complex activation involving

101   shifting of its six Fc-binding C1q subcomponents into a regular hexagonal configuration (**Fig. 2A, 3A**)

102   (12, 13). We therefore hypothesized that 34-1-2S assembles into hexamers on the pulmonary

103   endothelial surface of susceptible mice to trigger complement-dependent acute lung injury.

104   Imaging methods cannot currently resolve IgG hexamers in vivo, but recent studies have developed

105   methods for inhibiting IgG hexamerization. One approach to impair IgG hexamer assembly is to

106   carbamylate antibodies, converting lysine residues to homocitrullines to alter charge densities in IgG Fc

107   regions, inhibiting Fc:Fc interactions and IgG hexamer assembly (**Fig. 3B**) (23). Mice treated with

108   carbamylated 34-1-2S showed greatly reduced acute lung injury responses compared to littermate

109   controls treated with non-carbamylated 34-1-2S (**Fig. 3C, D**). Carbamylated 34-1-2S was deposited in

110   lungs but, in contrast to unchanged 34-1-2S, did not induce complement C3b/d deposition in the

111   pulmonary microvasculature (**Fig. 3E**)

112   Lysine residues are present on regions of IgG outside of the Fc:Fc interaction interface (illustrated in
113   **Fig. 3B**), so we pursued a more targeted strategy for inhibition of IgG hexamer assembly. We
114   determined the sequence of both heavy and light chain complementary-determining regions and
115   engineered a chimeric antibody with the Fab domain of 34-1-2S fused in frame to human IgG1 (hIgG1-
116   34-1-2S). To test whether hIgG1-34-1-2S causes injury through hexamerization, we also expressed this
117   antibody with an Fc point mutation that inhibits Fc:Fc interactions required for IgG hexamer assembly
118   (K439E, **Fig. 3F**) (15). hIgG1-34-1-2S caused acute lung injury that was reduced by the K439E
119   mutation (**Fig. 3G, H**), as was complement C4b/d deposition in lungs (**Fig 3I**), lending further support to
120   a role for Fc:Fc interactions and hexamerization in the pathogenesis of this disease model.

121   We also tested a strategy for pharmacologic inhibition of Fc:Fc interactions by mixing hIgG1-34-1-2S
122   with recombinant B domains from *Staphylococcus aureus* protein A (SpA-B), which bind to IgG
123   antibodies near to Fc:Fc interaction sites and inhibit hexamer assembly and complement activation by
124   antibodies targeting bacterial antigens (**Fig. 3J**) (17, 24). We hypothesized that these properties of
125   SpA-B, which likely evolved as part of an immune evasion strategy, might be harnessed to prevent
126   hIgG1-34-1-2S from causing acute lung injury. Adding SpA-B to hIgG1-34-1-2S reduced its ability to
127   both induce acute lung injury (**Fig. 3K, L**) and cause complement C4b/d deposition within pulmonary
128   arterioles (**Fig. 3M**). These findings provide a third line of evidence that Fc:Fc interactions leading to
129   hexamer assembly are important for the injury response caused by this alloantibody.

130   Turning to hexamer gain of function experiments, the introduction of three mutations into the Fc domain
131   of hIgG1 (RGY mutations: E345R, E430G, S440Y) resulted in antibodies capable of off-target hexamer
132   assembly as well as increased on-target hexamerization (15) (**Fig. 4A**). We hypothesized that RGY-
133   mutated 34-1-2S (RGY-hIgG1-34-1-2S) would have enhanced ability to cause acute lung injury due to
134   increased IgG hexamer formation. We produced RGY-hIgG1-34-1-2S and confirmed its ability to
135   spontaneously assemble into hexamers in solution (**Fig. 4B**). Consistent with a role for alloantibody
136   hexamerization in driving injury, RGY-hIgG1-34-1-2S showed increased potency in triggering acute
137   lung injury relative to hIgG1-34-1-2S (**Fig. 4C, D**), and inducing complement C4b/d deposition in lungs
138   (**Fig. 4E**). A novel chimeric hIgG1 antibody binding a single MHC class I antigen (hIgG1-Kd1, targeting
139   K^d), did not provoke injury when injected into B6.$H2^d$ mice (**Fig. 4F, G**), consistent with binding to
140   multiple antigens being a requirement for alloantibody-mediated acute lung injury. However,
141   introduction of the RGY mutations promoting hexamerization into this innocuous antibody resulted in a
142   modified version (RGY-hIgG1-Kd1) that was able to provoke increases in lung vascular permeability
143   and edema (**Fig. 4F & G**). Promoting IgG hexamer assembly can therefore increase in vivo
144   pathogenicity of alloantibodies.

145   Another approach for therapeutic exploitation of IgG hexamerization involves use of Fc hexamers as

146   'decoy' treatments. These therapeutic candidates are under investigation as recombinant alternatives to

147   plasma-derived intravenous or subcutaneous immunoglobulin (IVIg or SCIg) treatments that are used in

148   management of autoimmune and alloimmune diseases (25). We hypothesized that due to its ability to

149   inhibit classical complement activation (11, 26), the Fc hexamer 'decoy' treatment CSL777 (previously

150   Fc-μTP-L309C) would be effective in preventing alloantibody-mediated acute lung injury.

151   We randomized mice to receive either CSL777, SCIg (IgPro20, a human plasma-derived

152   immunoglobulin product which is currently used to treat antibody-mediated diseases), or vehicle

153   controls prior to injection with 34-1-2S (**Fig. 5A, B**). Treatment with CSL777 protected mice from

154   developing 34-1-2S-induced lung vascular permeability and pulmonary edema responses at all doses

155   tested, whereas treatment with SCIg only had a partial effect on alloantibody-induced acute lung injury

156   responses (**Fig. 5C-F**). CSL777 treated mice lacked alloantibody-mediated deposition of complement

157   C4 split products on pulmonary arterioles, whereas arteriolar endothelial C4b/d deposition was still

158   observed in lungs of SCIg-treated mice after 34-1-2S antibody injections (**Fig. 5G, H**). Recombinant Fc

159   hexamer therapeutics such as CSL777 might therefore be useful for prevention or treatment of

160   complement-dependent forms of alloantibody-mediated organ injury.

161   Unlike humans, mice do not express the Fcγ receptor FCGR2A (FcγRIIA, CD32A), negatively

162   impacting the predictive value of mouse models for studying human antibody-mediated diseases (27,

163   28). To test whether our previous findings held up in a system involving FCGR2A-driven pathology, we

164   crossed existing mouse lines to generate 34-1-2S-mediated injury-susceptible H-2^d mice expressing a

165   human FCGR2A (hFCGR2A) transgene (B6.$H2^d$:$hFCGR2A^{Tg/0}$). Mice expressing hFCGR2A developed

166   similar levels of lung injury relative to littermates without hFCGR2A expression but displayed a survival

167   disadvantage (**Fig. 6A-C**), and increased sequestration of platelets in the pulmonary microvasculature

168   (**Fig. 6D,E**). Classical complement activation was still critical for pathogenesis in the presence of

169   hFCGR2A, as knockout of *C1qa* protected mice expressing hFCGR2A from lung injury and mortality

170   (**Fig. 6F-H**). B6.$H2^d$:$hFCGR2A^{Tg/0}$ mice treated with CSL777 were protected from 34-1-2S-mediated

171   injury and showed no mortality responses (**Fig. 6I-K**). These results provide evidence that in a

172   humanized antibody-mediated acute lung injury model involving pathology driven by hFCGR2A,

173   classical complement activation is still a critical event in pathogenesis that can be targeted by

174   therapeutics.

Discussion

175

176 This study advances our understanding of immunology in three areas. Our work elucidates the

177 molecular determinants of susceptibility in a widely used inflammation model. To our knowledge, our

178 experiments represent the first in vivo evidence that alloantibody hexamerization is important for

179 pathophysiology. In addition, we show that two experimental therapeutic approaches that target

180 antibody hexamerization can prevent alloantibody-mediated organ injury.

181 The findings presented in this study allow us to explain a long-standing mystery of great mechanistic

182 importance in a widely used model of immune-mediated organ injury; in particular, why 34-1-2S

183 antibody injections (but not injections of other anti-MHC class I antibodies) cause such striking

184 pathophysiology in mice carrying the H-2^d but not H-2^b MHC haplotype (6, 19, 20, 28–38). We posit that

185 high affinity binding to multiple MHC class I antigens on the pulmonary endothelium of mice with the H-

186 2^d haplotype facilitates sufficiently dense alloantibody deposition for IgG hexamer assembly to occur.

187 These IgG hexamers then direct classical complement activation onto the pulmonary endothelial

188 surface, initiating the excessive leukocyte and platelet responses that have been reported in previous

189 studies to cause acute lung injury in this model (6, 19, 20). Furthermore, we were able to render an

190 innocuous antibody specific for a single MHC class I antigen into a pathogenic antibody by introducing

191 mutations promoting increased on and off-target hexamerization. An additional implication of our

192 findings is that both lymphocyte crossmatch and single antigen bead assays for detecting complement-

193 fixing antibodies may lack sensitivity for detecting antibodies that activate complement in vivo. The

194 mobility, density and diversity of antigens on the lymphocytes or solid-phase beads used in these

195 assays does not exactly resemble those on endothelial cell surfaces targeted by donor-specific

196 antibodies in vivo, and our results indicate that each of these factors determines complement-fixing

197 capability of antibodies. Conversely, antigen density on beads exceeding that found in vivo may give

198 false positive findings of complement-fixing antibody responses.

199 By demonstrating that IgG hexamers are important in pathophysiology and represent therapeutic

200 targets in vivo, our work builds on in vitro studies implicating antibody hexamerization in complement

201 activation by antibodies targeting antigens on liposomes, lymphoma cells or bacterial membranes (15–

202 18, 23, 39). Further clinical translation will require determination of the importance of IgG hexamers in

203 more complex models of diseases involving complement-activating alloantibodies (e.g. AbMR, TRALI,

204 hemolytic transfusion reactions, and hemolytic disease of the fetus and newborn) or autoantibodies

205 (e.g. warm autoimmune hemolytic anemia, antiphospholipid syndrome, myasthenia gravis and

206 neuromyelitis optica). As SpA-B does not inhibit IgG3-mediated complement activation but IgG3 can

207 assemble into hexamers (15, 16), it will also be important to develop strategies to inhibit IgG3

208 hexamerization to examine the therapeutic potential of targeting hexamers formed by IgG3 antibodies.

209 Our results also provide new insights into the modes of action of past, present, and potential future

210 therapeutics. Full length staphylococcal protein A (SpA) has been used as a therapeutic in the form of a

211 now-discontinued extracorporeal immunoadsorption product (Prosorba column). Efficacy of SpA

212 immunoadsorption has been observed in patients with symptoms unchanged by plasma exchange, an

213 effect ascribed to leakage of SpA from columns into the bloodstreams of patients resulting in B cell

214 depletion caused by the action of SpA as a B cell receptor super agonist (40). Purified SpA infusions

215 (PRTX-100) were subsequently studied in early-stage clinical trials before abandonment for financial

216 reasons (41). Our results suggest that there may be settings where therapeutics based on the SpA-B

217 subdomain of SpA have efficacy through preventing complement activation without risk of adverse

218 effects related to immune complex formation and B cell super agonism caused by immunoglobulin

219 polyvalency of full-length SpA. Donor-derived immunoglobulin products (e.g. IVIg and SCIg) are

220 currently used to treat antibody-mediated disease flares. Our observation that SCIg reduces injury

221 responses but does not prevent classical complement activation in vivo is concordant with previous

222 studies concluding that immunoglobulin therapeutics act on downstream mediators in vitro and in vivo

223 (33, 42). CSL777 is an attractive potential future therapeutic for treatment of alloantibody-mediated

224 diseases as it showed efficacy in our models, and had a mode of action that would be anticipated to

225 prevent complement activation by both IgM and IgG antibodies as well as pathophysiology resulting

226 from Fcγ receptors (11, 25, 26). CSL777 also lacks issues with use of donor-derived products related to

227 sourcing, purification and concentration for injections (25, 43).

228 In conclusion, this study provides evidence that IgG hexamers can be important triggers of

229 complement-dependent pathophysiology in vivo. Our preclinical studies support further investigation of

230 IgG hexamerization inhibitors and IgG hexamer 'decoy' therapeutics for use in preventing disease

231 states caused by antibodies and complement activation.

Materials and methods

Animals

B6.C-*H2^d*/bByJ (B6.*H2^d*) mice (Cat# 000359) (44) and B6(Cg)-*C1qa$^{tm1d(EUCOMM)Wtsi}$*/TennJ (*C1qa$^{-/-}$*) mice (Cat# 031675) (22) originated from the Jackson Laboratory. B6-background mice were bred with B6.*H2^d* mice and progeny were crossed to produce mice with homozygous expression of H2^d MHC antigens for use in experiments (6). B6.ConK^d-on and B6.Tg(CD2-Tcra,-Tcrb)75Bucy (TCR75) mice were provided by J. Zimring (21, 45). BALB/c mice were from Charles River Laboratories (Cat# 028). B6;SJL-Tg(FCGR2A)11Mkz/J mice (expressing human FCGR2A isoform R131, Jackson Laboratory Cat# 003542) (27) were backcrossed to B6 congenicity (46). Male mice were used as female mice are not susceptible to 34-1-2S-mediated injury (5). Mice were studied at 8-16 weeks of age after maintenance in the UCSF specific pathogen-free animal facility for at least 2 weeks. Procedures received ethical approval from the UCSF IACUC committee.

Surface plasmon resonance

Binding affinities were determined by injecting serial dilutions (0.5-200 nM) of MHC class I monomers (MBL International Cat#: TB-5001-M (K^b presenting SIINFEKL); TB-5008-M (D^b presenting RAHYNIVTF); TB-M552-M (K^d presenting VYLKTNVFL); TB-M536-M (D^d presenting IGPGRAFYA); TB-M521-M (L^d presenting SPSYVYHQF)) over monoclonal antibodies bound via amine coupling to SensEye G Easy2Spot sensors (Ssens Cat# 1-09-04-006), assayed in triplicate with an IBIS MX96 SPR imager.

Alloantibody-mediated acute lung injury model

As previously described, mice were given i.p. injections of LPS (Sigma Aldrich Cat# L2880, 0.1 mg/kg) for 'priming' needed to render barrier-housed mice responsive to antibody injections (19). At 24 hours after LPS priming, mice were anesthetized (0.6 mg/kg ketamine + 0.1 mg/kg xylazine i.p.) and the indicated antibody treatments were injected into the jugular vein over the course of 1 minute (at 1 mg/kg unless otherwise stated). Antibodies were from BioXCell (mIgG2a isotype control Cat# BE0085, 34-1-2S Cat# BE0180, hIgG1 isotype control Cat# BE0297) or newly produced (described below). Lung vascular permeability was measured by giving each mouse 0.01 KBq of ^{131}I-conjugated albumin (Iso-Tex Diagnostics, NDC:50914-7731) together with i.v. antibody injections, collecting lungs and blood samples 2 hours later or at cessation of breathing for radioactivity measurements used to quantity volume of extravasated plasma in lungs (lung vascular permeability). Wet-dry weight ratios of lungs and blood were used to calculate excess lung water volumes (6).

263 *Immunofluorescence imaging*

264 Cryosections were made at 200 μm or 400 μm thickness from lungs fixed by inflation with and

265 immersion in 1% formaldehyde in PBS, as previously described (6). Sections were incubated overnight

266 with antibodies targeting C3b/d (Novus Cat# NB200-540), C1qa (Abcam Cat# ab182451), C4b/d

267 (Novus Cat# NB200-541), Scgb1a1 (Sigma Aldrich Cat# ABS1673) or CD41 (Biolegend Cat# 133939)

268 together with a FITC-conjugated antibody raised against Acta2 (Sigma-Aldrich Cat# F3777) were

269 incubated overnight at 1:500 with 5% normal donkey serum, 0.1% bovine serum albumin and 0.3%

270 triton X-100 in phosphate-buffered saline (PBS). After washing, Cy3 or Alexa Fluor 647-conjugated

271 cross-adsorbed polyclonal secondary antibodies targeting rat, rabbit, goat and/or mouse IgG (Jackson

272 Immunoresearch Cat# 712-165-153, Cat# 711-165-152, Cat# 705-605-147 and/or Cat# 115-605-206)

273 were incubated with sections at 1:500 in PBS + 0.3% triton X-100 overnight. After additional washes,

274 sections were either mounted in Vectashield (Vector Laboratories Cat# H-1700) for standard confocal

275 imaging on a Nikon A1r microscope, or cleared after staining using the EZ clear protocol (47) for 3D

276 imaging with a Nikon AZ100M confocal microscope.

277 *Antibody carbamylation*

278 Carbamylation of 34-1-2S was achieved by incubating 1 mg of antibody in PBS + 0.1 M KOCN for 1

279 hour at 37°C before buffer exchange back into PBS (23). Control 34-1-2S was subjected to the same

280 process with omission of KOCN.

281 *Antibody sequencing and engineering*

282 The 34-1-2S hybridoma was purchased from ATCC (Cat# HB-79). To generate the Kd1 hybridoma, B6

283 mice were injected i.v. with $3×10^6$ CD4+ T cells from TCR75 mice transgenic for a T cell receptor (TCR)

284 specific for a peptide from K^d presented by IA^b, and i.p. with $5×10^6$ Con-K^d-on splenocytes, resulting in

285 an extreme B cell antibody response directed at an immunodominant peptide from K^d, the only

286 mismatched antigen between donor and recipient. Three days after a boost with an additional i.p.

287 injection with Con-K^d-on splenocytes, splenocytes from the sensitized recipient were fused with a

288 myeloma cell line as previously described (48), and monoclonal antibodies specific for K^d were

289 identified using Con-K^d-on splenocytes as targets (21).

290 Monoclonal antibody aliquots were digested with either peptidyl-Asp metalloendopeptidase,

291 chymotrypsin, elastase, trypsin, or pepsin enzymes. Peptides were then assayed using liquid

292 chromatography coupled to tandem mass spectrometry for sequencing of variable fragments

293 (Bioinformatics Solutions Inc.). Amino acid sequences determined were, for 34-1-2S:

294 EVQLQQSGAEFVRPGASVKLSCTASGFNLKDDYMFWVKQRPEQGLEWIGWIAPDNGDTEYASKFQG

295 KATITADTSSNTAYVQLSSLTSEDTAVYYCTTWGYYSYVNYWGQGTTLTVSS (heavy chain variable

296 region) and:

297 DIQMTQSPSSLSASLGERVSLTCRASQDIGSNLNWLQQEPDGTIKRLIYATYSLDSGVPKRFSGSRSGS

298 DYSLTISSLESEDFVDYYCLQYASSPYTFGGGTKLEIK (light chain variable region); and for Kd1:

299 EVLLVESGGDLVKPGGSLKLSCAASGFTFRTYAMSWVRQTPEKRLEWVATIGDDGSYTFYPDNVKGR

300 FTISRDNAKNNLYLQMRHLKSEDTAIYFCARDGLFAYWGQGTLVTVSA (heavy chain variable region)

301 and:

302 DIQMTQSPSSLSASLGGKVTITCKASQDIKKNIAWYQYKPGKGPRLLIHYTSTLQPGISSRFSGSGSGR

303 DYSFSISNLEPEDIATYYCLQYDSLLYTFGGGTKLEIK (light chain variable region). Correct

304 identification of variable domains was confirmed by performing sequencing of the products of 5' rapid

305 amplification of cDNA ends (5'-RACE) for heavy and light chain mRNA using RNA isolated from

306 hybridomas. The isolated 5'-RACE amplicons contained open reading frames that encoded the above

307 peptides sequenced by mass spectrometry. These sequences were codon-optimized and antibodies

308 were expressed as chimeric hIgG1 with or without Fc point mutations in a HEK293 cell system and

309 purified using protein A and buffer exchange (Absolute Antibody).

310 *Pharmacologic treatments*

311 Recombinant subdomain B from Staphylococcus aureus (SpA-B, amino acid sequence:

312 HHHHHHADNKFNKEQQNAFYEILHLPNLNEEQRNGFIQSLKDDPSQSANLLAEAKKLNDAQAPK, His-

313 tag added for purification) was produced in an *E. coli* system by Genscript and supplied in protein

314 storage buffer (50 mM Tris-HCl, 150 mM NaCl, 10% Glycerol, pH 8.0). At 1-2 hours before i.v. injection,

315 SpA-B (3 mg/kg) or vehicle were mixed with hIgG1-34-1-2S resulting in a 30% vehicle, 70% PBS

316 mixture.

317 Trial formulations of CSL777 (in PBS vehicle), as well as clinical-grade IgPro20 (Hizentra™) and the

318 proprietary vehicle for IgPro20 were provided by CSL Behring. Mice were given i.p. injections of

319 CSL777, IgPro20 or relevant vehicle 1-2 hours before i.v. injections of antibodies at stated doses.

320 *Negative stain electron microscopy*

321 Antibody samples were diluted to 0.01 mg/ml in 25 mM HEPES, 100 mM NaCl and added to carbon-

322 coated grids (TedPella Cat# 01702-F, manually coated with 20 nm carbon using a Cressington 208

323 Sputter Coater). Sample-coated grids were stained using 0.75% uranyl formate and imaged on an FEI

324 Tecnai T12 transmission electron microscope.

Experimental design and analysis

Within-cage randomization was used for group allocations in studies testing exogenous treatments. Littermate controls from heterozygous crosses were used to test the effect of *C1qa* knockout. Congenic animals housed in the same room were used to study haplotype effects. Handlers were blinded to group allocations during experiments. Group numbers (n) and analysis approaches were predetermined before initiation of experiments. Statistical tests used on each dataset are described in figure legends.

Software

GraphPad Prism was used for graphing and statistical analysis. UCSF ChimeraX was used for molecular graphics (49). Imaris was used to render fluorescence micrographs and ImageJ was used to process electron microscopy data.

Authorship

347 Conceptualization: SJC, JCZ, MRL

348 Methodology: SJC, MRL, AEHB, GV, ÉB, RS, JCZ

349 Investigation: SJC, YS, JJT, NK, DPB, AEHB

350 Funding acquisition: SJC, JCZ, MRL

351 Writing – original draft: SJC, MRL

352 Writing – review & editing: SJC, YS, JJT, NK, DPB, AEHB, GV, ÉB, RS, JCZ, MRL

353 Conflict of interest statement: RS is an employee of CSL Behring AG, Switzerland. The authors have

354 no additional conflicts of interest.

Data and materials availability

356 All data are available in the main text or the supplementary materials.

Supplementary materials

358 Supplementary materials and methods.

359 Supplementary Figures:

360 **Fig. S1. Binding of MHC class I monoclonal antibodies to MHC class I monomers.**

361 **Movie S1. Complement C4 split product deposition in the pulmonary vasculature.**
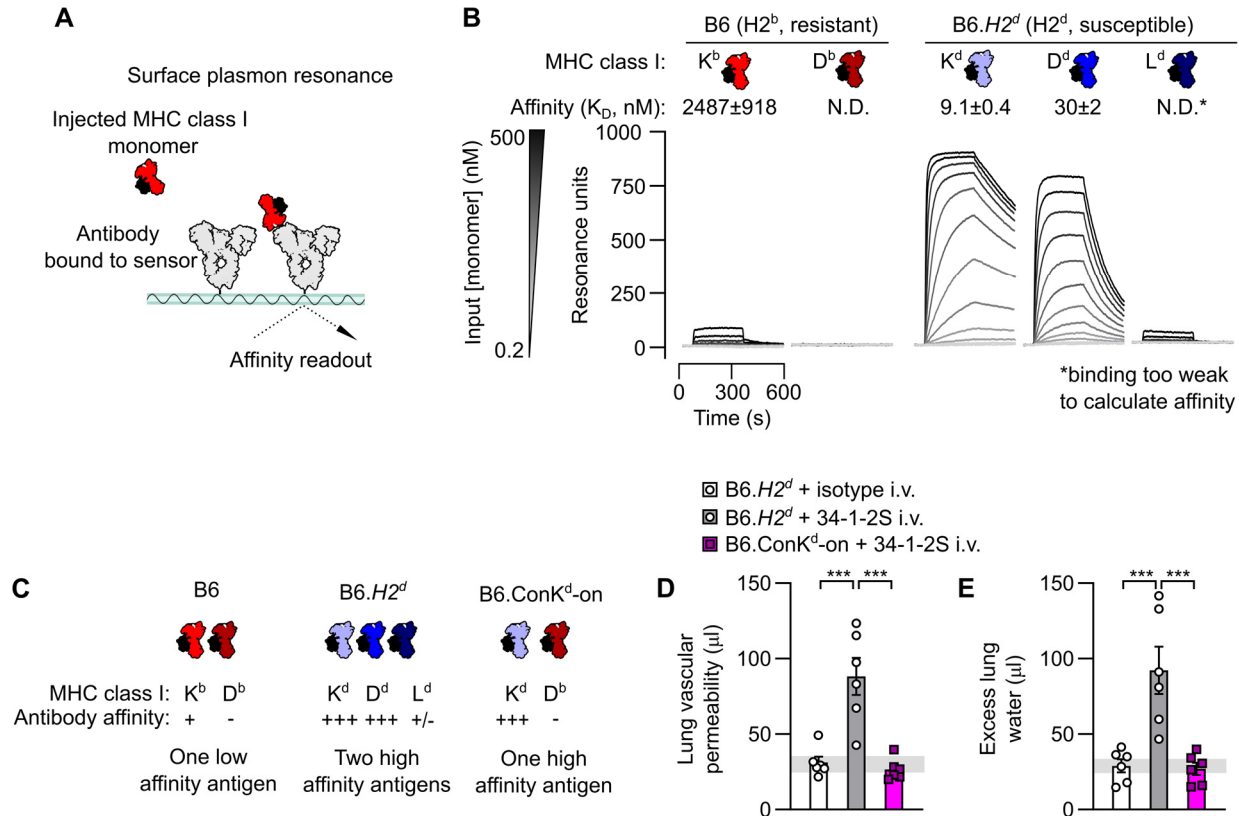
362 **References**

363 1. Vlaar APJ, Juffermans NP. Transfusion-related acute lung injury: a clinical review. *Lancet*.
364 2013;382(9896):984–994.

365 2. Panch SR, Montemayor-Garcia C, Klein HG. Hemolytic Transfusion Reactions. *New England Journal*
366 *of Medicine*. 2019;381(2):150–162.

367 3. Loupy A, Lefaucheur C. Antibody-Mediated Rejection of Solid-Organ Allografts. *New England*
368 *Journal of Medicine*. 2018;379(12):1150–1160.

369 4. Delaney M, Matthews DC. Hemolytic disease of the fetus and newborn: managing the mother, fetus,
370 and newborn. *Hematology*. 2015;2015(1):146–151.

371 5. Strait RT, et al. MHC class I-specific antibody binding to nonhematopoietic cells drives complement
372 activation to induce transfusion-related acute lung injury in mice. *The Journal of experimental medicine*.
373 2011;208(12):2525–2544.

374 6. Cleary SJ, et al. Complement activation on endothelium initiates antibody-mediated acute lung injury.
375 *The Journal of Clinical Investigation*. [published online ahead of print: July 30, 2020].
376 https://doi.org/10.1172/JCI138136.

377 7. Toy P, et al. Transfusion-related acute lung injury: Incidence and risk factors. *Blood*.
378 2012;119(7):1757–1767.

379 8. Bouquegneau A, et al. Complement-activating donor-specific anti-HLA antibodies and solid organ
380 transplant survival: A systematic review and meta-analysis. *PLoS Medicine*. 2018;15(5).
381 https://doi.org/10.1371/journal.pmed.1002572.

382 9. Berentsen S, Barcellini W. Autoimmune Hemolytic Anemias. *New England Journal of Medicine*.
383 2021;385(15):1407–1419.

384 10. Chen M, Jayne DRW, Zhao M-H. Complement in ANCA-associated vasculitis: mechanisms and
385 implications for management. *Nat Rev Nephrol*. 2017;13(6):359–367.

386 11. Tradtrantip L, et al. Recombinant IgG1 Fc hexamers block cytotoxicity and pathological changes in
387 experimental in vitro and rat models of neuromyelitis optica. *Neuropharmacology*. 2018;133:345–353.

388 12. Mortensen SA, et al. Structure and activation of C1, the complex initiating the classical pathway of
389 the complement cascade. *Proceedings of the National Academy of Sciences*. 2017;114(5):986–991.

390 13. Sharp TH, et al. Insights into IgM-mediated complement activation based on in situ structures of
391 IgM-C1-C4b. *Proceedings of the National Academy of Sciences*. 2019;116(24):11900–11905.

392 14. Burton DR. Antibody: the flexible adaptor molecule. *Trends in Biochemical Sciences*.
393 1990;15(2):64–69.

394 15. Diebolder CA, et al. Complement is activated by IgG hexamers assembled at the cell surface.
395 *Science*. 2014;343(6176):1260–1263.

396   16. Abendstein L, et al. Complement is activated by elevated IgG3 hexameric platforms and deposits
397   C4b onto distinct antibody domains. *Nat Commun*. 2023;14(1):4027.

398   17. Cruz AR, et al. Staphylococcal protein A inhibits complement activation by interfering with IgG
399   hexamer formation. *Proc Natl Acad Sci U S A*. 2021;118(7):e2016772118.

400   18. de Jong RN, et al. A Novel Platform for the Potentiation of Therapeutic Antibodies Based on
401   Antigen-Dependent Formation of IgG Hexamers at the Cell Surface. *PLoS Biol*. 2016;14(1):e1002344.

402   19. Looney MR, et al. Platelet depletion and aspirin treatment protect mice in a two-event model of
403   transfusion-related acute lung injury. *Journal of Clinical Investigation*. 2009;119(11):3450–3461.

404   20. Looney MR, et al. Neutrophils and their Fc gamma receptors are essential in a mouse model of
405   transfusion-related acute lung injury. *The Journal of clinical investigation*. 2006;116(6):1615–23.

406   21. Hudson KE, et al. Alloimmunogenicity of an isolated MHC allele is affected by the context of MHC
407   mismatch in a murine model. *Transfusion*. 2019;59(2):744–753.

408   22. Fonseca MI, et al. Cell-specific deletion of C1qa identifies microglia as the dominant source of C1q
409   in mouse brain. *J Neuroinflammation*. 2017;14(1):48.

410   23. Lubbers R, et al. Carbamylation reduces the capacity of IgG for hexamerization and complement
411   activation. *Clinical and Experimental Immunology*. 2020;200(1):1–11.

412   24. Ultsch M, et al. 3-2-1: Structural insights from stepwise shrinkage of a three-helix Fc-binding
413   domain to a single helix. *Protein Engineering, Design and Selection*. 2017;30(9):619–625.

414   25. Zuercher AW, et al. Next-generation Fc receptor–targeting biologics for autoimmune diseases.
415   *Autoimmunity Reviews*. 2019;18(10):102366.

416   26. Spirig R, et al. rIgG1 Fc Hexamer Inhibits Antibody-Mediated Autoimmune Disease via Effects on
417   Complement and FcγRs. *The Journal of Immunology*. 2018;200(8):2542–2553.

418   27. McKenzie SE, et al. The Role of the Human Fc Receptor FcγRIIA in the Immune Clearance of
419   Platelets: A Transgenic Mouse Model. *The Journal of Immunology*. 1999;162(7).

420   28. El Mdawar MB, et al. Platelet FcγRIIA-induced serotonin release exacerbates the severity of
421   transfusion-related acute lung injury in mice. *Blood advances*. 2021;5(23):4817–4830.

422   29. Mallavia B, et al. Mirasol pathogen reduction technology treatment of human whole blood does not
423   induce acute lung injury in mice. *PLOS ONE*. 2017;12(6):e0178725.

424   30. Hidalgo A, et al. Heterotypic interactions enabled by polarized neutrophil microdomains mediate
425   thromboinflammatory injury. *Nat Med*. 2009;15(4):384–391.

426   31. Adrover JM, et al. Programmed 'disarming' of the neutrophil proteome reduces the magnitude of
427   inflammation. *Nat Immunol*. 2020;21(2):135–144.

428   32. Song D, et al. PTP1B inhibitors protect against acute lung injury and regulate CXCR4 signaling in
429   neutrophils. *JCI Insight*. 2022;7(14). https://doi.org/10.1172/jci.insight.158199.

430 33. Semple JW, et al. Intravenous Immunoglobulin Prevents Murine Antibody-Mediated Acute Lung
431 Injury at the Level of Neutrophil Reactive Oxygen Species (ROS) Production. *PLoS One*.
432 2012;7(2):e31357.

433 34. Hechler B, et al. Platelets are dispensable for antibody-mediated transfusion-related acute lung
434 injury in the mouse. *Journal of Thrombosis and Haemostasis*. 2016;14(6):1255–1267.

435 35. McKenzie CGJ, et al. Peripheral blood monocyte-derived chemokine blockade prevents murine
436 transfusion-related acute lung injury (TRALI). *Blood*. 2014;123(22):3496–3503.

437 36. Sreeramkumar V, et al. Neutrophils scan for activated platelets to initiate inflammation. *Science*.
438 2014;346(6214):1234–8.

439 37. Caudrillier A, et al. Platelets induce neutrophil extracellular traps in transfusion-related acute lung
440 injury. *J Clin Invest*. 2012;122(7):2661–2671.

441 38. Ortiz-Muñoz G, et al. Aspirin-triggered 15-epi-lipoxin A4 regulates neutrophil-platelet aggregation
442 and attenuates acute lung injury in mice. *Blood*. 2014;124(17):2625–34.

443 39. Strasser J, et al. Unraveling the Macromolecular Pathways of IgG Oligomerization and Complement
444 Activation on Antigenic Surfaces. *Nano Lett*. 2019;19(7):4787–4796.

445 40. Silverman GJ, Goodyear CS, Siegel DL. On the mechanism of staphylococcal protein A
446 immunomodulation. *Transfusion*. 2005;45(2):274–280.

447 41. Bussel JB, et al. Safety and Efficacy of PRTX-100, a Highly Purified Form of Staphylococcal Protein
448 A, in Patients with Immune Thrombocytopenia (ITP). *Blood*. 2016;128(22):4929.

449 42. Basta M, Fries LF, Frank MM. High doses of intravenous immunoglobulin do not affect the
450 recognition phase of the classical complement pathway. *Blood*. 1991;78(3):700–702.

451 43. Shock A, Humphreys D, Nimmerjahn F. Dissecting the mechanism of action of intravenous
452 immunoglobulin in human autoimmune disease: Lessons from therapeutic modalities targeting Fcγ
453 receptors. *Journal of Allergy and Clinical Immunology*. 2020;146(3):492–500.

454 44. Bailey DW. Genetics of histocompatibility in mice. *Immunogenetics*. 1975;2(1):249–256.

455 45. Honjo K, et al. Evidence for cooperativity in the rejection of cardiac grafts mediated by CD4 TCR Tg
456 T cells specific for a defined allopeptide. *Am J Transplant*. 2004;4(11):1762–1768.

457 46. Cloutier N, et al. Platelets release pathogenic serotonin and return to circulation after immune
458 complex-mediated sequestration. *Proceedings of the National Academy of Sciences of the United
459 States of America*. 2018;115(7):E1550–E1559.

460 47. Hsu C-W, et al. EZ Clear for simple, rapid, and robust mouse whole organ clearing. *eLife*.
461 2022;11:e77419.

462 48. Howie HL, et al. Serological blind spots for variants of human IgG3 and IgG4 by a commonly used
463 anti-immunoglobulin reagent. *Transfusion*. 2016;56(12):2953–2962.

464 49. Goddard TD, et al. UCSF ChimeraX: Meeting modern challenges in visualization and analysis.
465 *Protein Sci*. 2018;27(1):14–25.

466   50. Yuan D, et al. Structure of IgG-Fc hexamer reveals a mutual lock-and-key mode of Fc-Fc
467   interaction [preprint]. 2022;2022.02.24.481884.

468

469

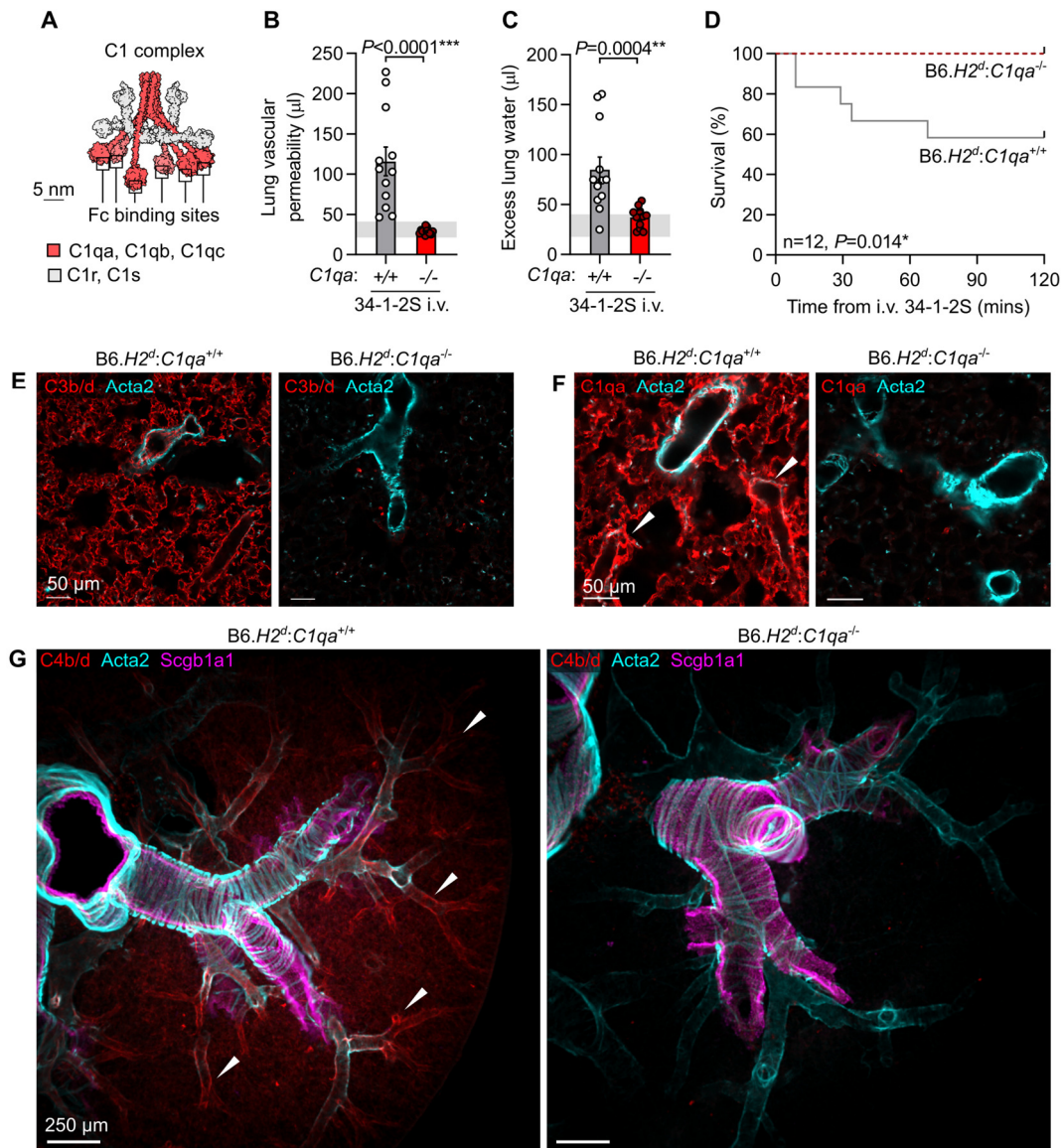**Fig. 1. The 34-1-2S alloantibody binds to multiple MHC class I antigens to trigger acute lung injury.**

A. Schematic showing approach for measuring affinity of the MHC class I alloantibody 34-1-2S for MHC class I monomers using surface plasmon resonance (SPR).

B. SPR sensorgrams showing detection of binding of 34-1-2S to the K^b MHC class I antigen from $H2^b$ mice and the K^d, D^d and L^d antigens from mice with the $H2^d$ haplotype.

C. Classical MHC class I antigens present in B6, B6.$H2^d$ and B6.Con-K^d-on mice with summary of results from **B**.

D. Lung vascular permeability and **E**. excess lung water measurements from LPS-primed B6.$H2^d$ mice given intravenous (i.v.) doses of either 34-1-2S or isotype control, versus B6.Con-K^d-on mice given i.v. 34-1-2S.

Depictions of IgG and MHC class I in **A-C** are based on protein data bank (PDB) entries 1HZH and 1RK1. **B, D & E** show means ± standard errors. Statistical tests used on **D & F** were ordinary one-way ANOVA with Dunnett's test for differences relative to B6.$H2^d$ + 34-1-2S i.v. group, with data $\log_{10}$-transformed prior to analysis, *** = $P<0.0001$.

Fig. 2. Classical complement activation on the pulmonary endothelium initiates 34-1-2S-induced acute lung injury.

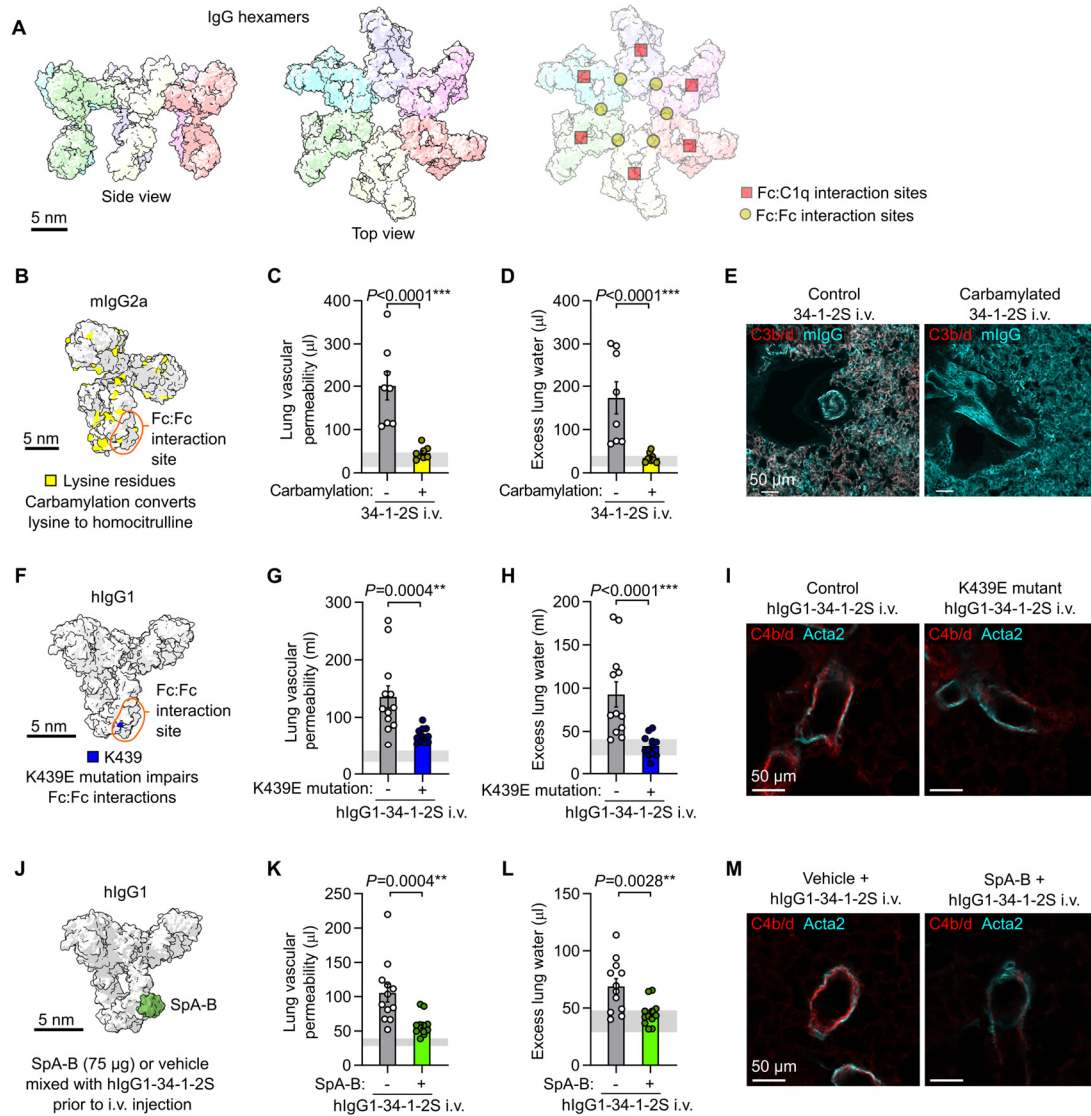**A**. Molecular model of C1 complex based on small angle scattering database entry SASDB38 (12).

B. Lung vascular permeability and **C**. excess lung water measurements from LPS-primed B6.$H2^d$:$C1qa^{-/-}$ mice and B6.$H2^d$:$C1qa^{+/+}$ littermates given i.v. 34-1-2S at 1 mg/kg. Horizontal gray lines are standard deviations of values from 'no injury' controls (B6.$H2^d$ mice given LPS i.p. + mIgG2a isotype control i.v.)

D. Survival of LPS-primed B6.$H2^d$:$C1qa^{-/-}$ mice and B6.$H2^d$:$C1qa^{+/+}$ littermates given i.v. 34-1-2S at 4.5 mg/kg.

E. Immunofluorescence staining for complement C3b/d, **F**. C1qa or **G**. C4b/d (red) as well as Acta2 (α-smooth muscle actin, cyan) and, in **G**., Scgb1a1 (club cell secretory protein, magenta) in lung sections from LPS-primed B6.$H2^d$:$C1qa^{-/-}$ mice and B6.$H2^d$:$C1qa^{+/+}$ mice fixed 5 minutes after i.v. 34-1-2S at 1 mg/kg. Images in **G**. are maximum intensity projections sampling 240 μm from a cleared thick section. White arrowheads point to arterioles positive for complement components.

B & **C** show means ± standard errors. *P*-values are from unpaired two-tailed t-tests on $\log_{10}$-transformed data (**B** & **C**) or log-rank test (**D**), with group n=12.

494

Fig. 3. Inhibiting IgG hexamer assembly reduces 34-1-2S-induced acute lung injury responses.

A. Molecular models of IgG hexamers based on PDB entry 1HZH, showing Fc:Fc and Fc:C1q interaction sites.

B. Molecular model showing lysine residues in mouse IgG2a (mIgG2a), PDB entry 1IGT.

C. Lung vascular permeability, **D**. excess lung water measurements and **E**. lung complement C3b/d and mIgG immunostains from LPS-primed BALB/c mice after i.v. injection of carbamylated or control 34-1-2S.
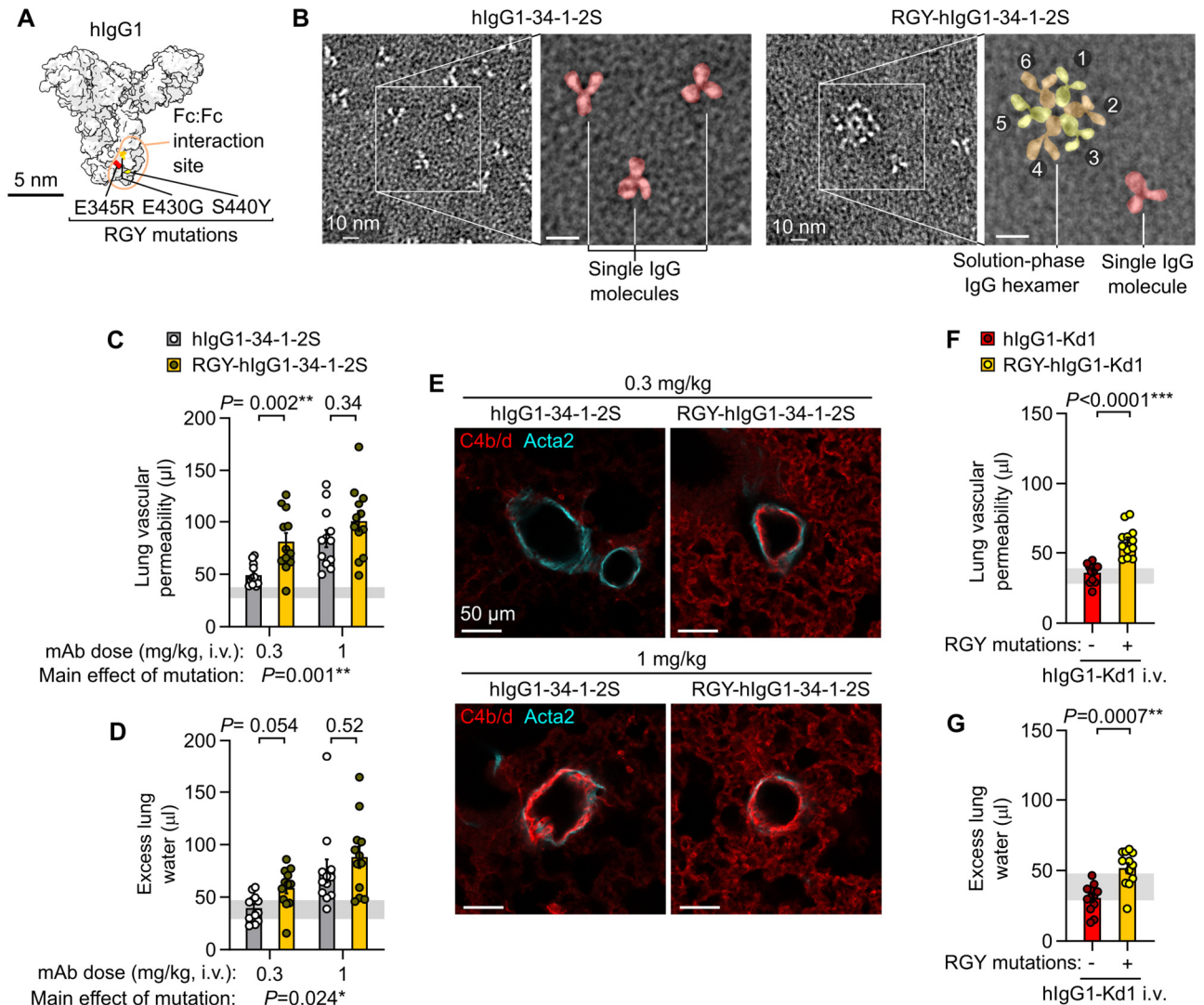
F. Molecular model showing location of Fc domain lysine 439 (K439) in human IgG1 (hIgG1), PDB entry 1HZH.

G. Lung vascular permeability, **H**. excess lung water measurements and **I**. lung complement C4b/d and Acta2 immunostains from LPS-primed B6.$H2^d$ mice after i.v. injection with hIgG1-34-1-2S or hIgG1-34-1-2S with K439E mutation.

J. Molecular model showing binding site of SpA-B to Fc domain of human IgG1 (hIgG1), PDB entries 1HZH and 5U4Y.

K. Lung vascular permeability, **L**. excess lung water measurements and **M**. lung complement C4b/d and Acta2 immunostains from LPS-primed B6.$H2^d$ mice after i.v. injection with hIgG1-34-1-2S either mixed with 75 μg SpA-B or vehicle control.

Samples for injury measurements were collected at 2 hours after antibody injections and lungs were fixed for immunostaining at 5 minutes after antibody injections. Graphs show means ± standard errors. P-values are from unpaired two-tailed t-tests on $\log_{10}$-transformed data, with group n=8 (**C**, **D**) or n=12 (**G**, **H**, **K**, **L**).

Page 21

Fig. 4. Fc mutations promoting IgG hexamer assembly increase in vivo pathogenicity of alloantibodies.

A. Molecular model showing amino acids mutated in RGY-hIgG1 antibodies, based on PDB entry 1HZH.

B. Negative stain electron micrographs showing single hIgG1-34-1-2S molecules and spontaneous solution-phase hexamers formed by RGY-hIgG1-34-1-2S (colored overlay highlights structures in expanded images).

C. Lung vascular permeability and **D**. excess lung water measurements from LPS-primed B6.$H2^d$ mice injected with control or RGY-mutated hIgG1-34-1-2S monoclonal antibodies (mAbs) at i.v. doses of either 0.3 or 1 mg/kg.

E. Immunofluorescence staining showing pulmonary arterioles stained for complement C4b/d (red) and Acta2 (cyan) in lung sections from LPS-primed B6.$H2^d$ mice given indicated treatments, with samples fixed 5 minutes after antibody injections.
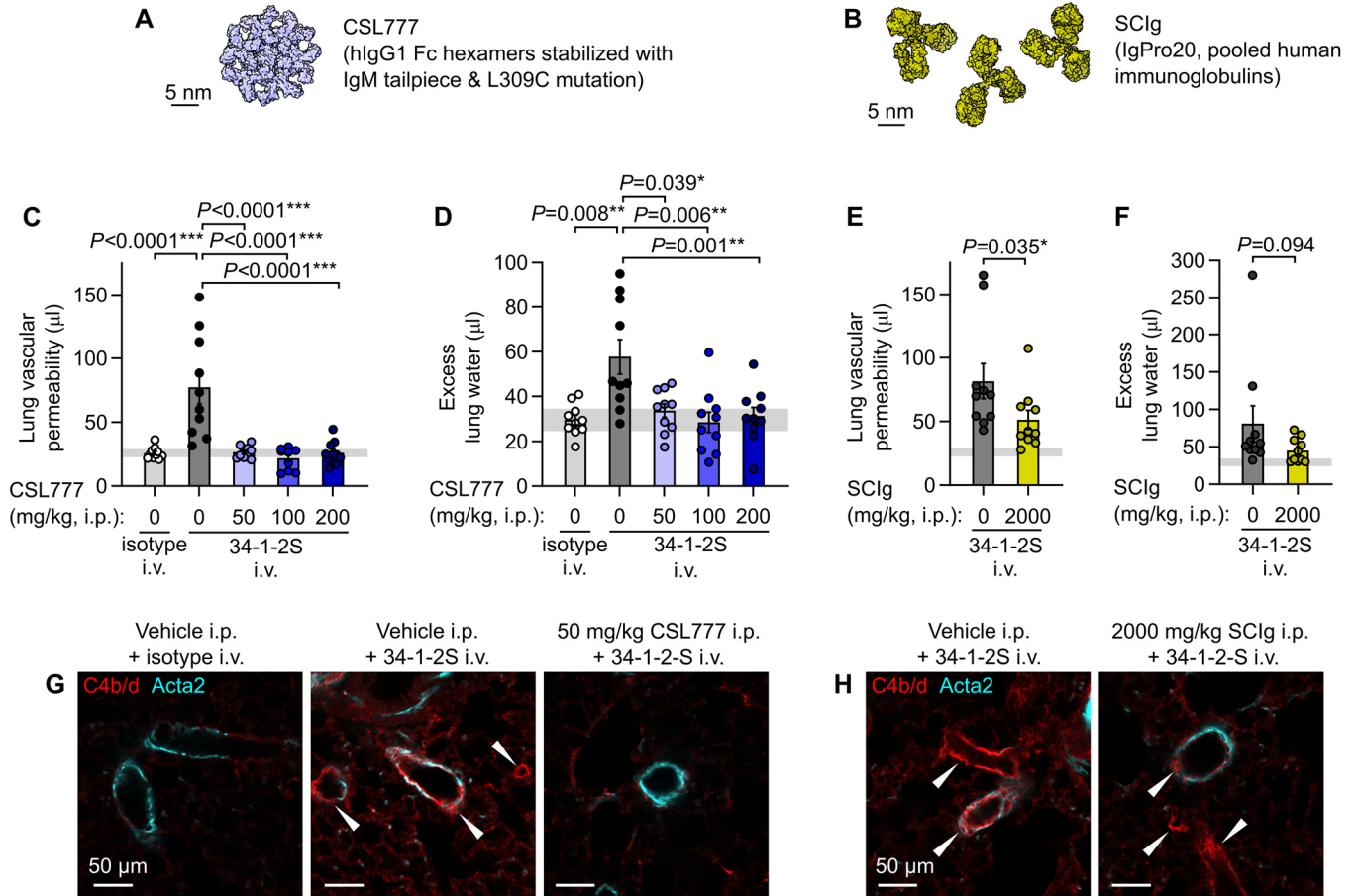
F. Lung vascular permeability and **G**. excess lung water measurements from LPS-primed B6.$H2^d$ mice injected with control or RGY-mutated hIgG1-Kd1 (a novel mAb targeting only the H-2K^d MHC class I antigen) at 1 mg/kg i.v..

Graphs show means ± standard errors with horizontal line representing standard deviations from 'no injury' controls (LPS-primed B6.$H2^d$ mice given hIgG1 isotype control i.v.). Log$_{10}$-transformed data were analyzed using an ordinary two-way ANOVA with Šídák's multiple comparisons test for effect of Fc mutation within dose level (**C, D**) or unpaired two-tailed t-test (**F, G**), with group n=12.

524

Fig. 5. Treatment with recombinant Fc hexamer decoys prevents alloantibody-mediated acute lung injury.

A. Molecular representation of CSL777, an investigational recombinant Fc hexamer 'decoy' treatment which inhibits classical complement activation, based on PDB entry 7X13 (50).

B. Molecular representation of SCIg, a pooled human immunoglobulin therapeutic with anti-inflammatory properties at high doses, based on PDB entry 1HZH.

C. Lung vascular permeability and **D**. excess lung water measurements from LPS-primed BALB/c mice given i.p. vehicle or CSL777 at indicated doses 1 hour before i.v. injection with 34-1-2S or mIgG2a isotype control.

E. Lung vascular permeability and **F**. excess lung water measurements from LPS-primed BALB/c mice given i.p. vehicle or 2000 mg/kg SCIg 1 hour before i.v. injection with 34-1-2S or mIgG2a isotype control.

G. and **H**. Immunofluorescence showing pulmonary arterioles stained for complement C4b/d (red) and Acta2 (cyan) in lung sections from LPS-primed BALB/c mice given indicated treatments, with samples fixed 5 minutes after antibody injections. White arrowheads point to arterioles with endothelial positivity for C4b/d.
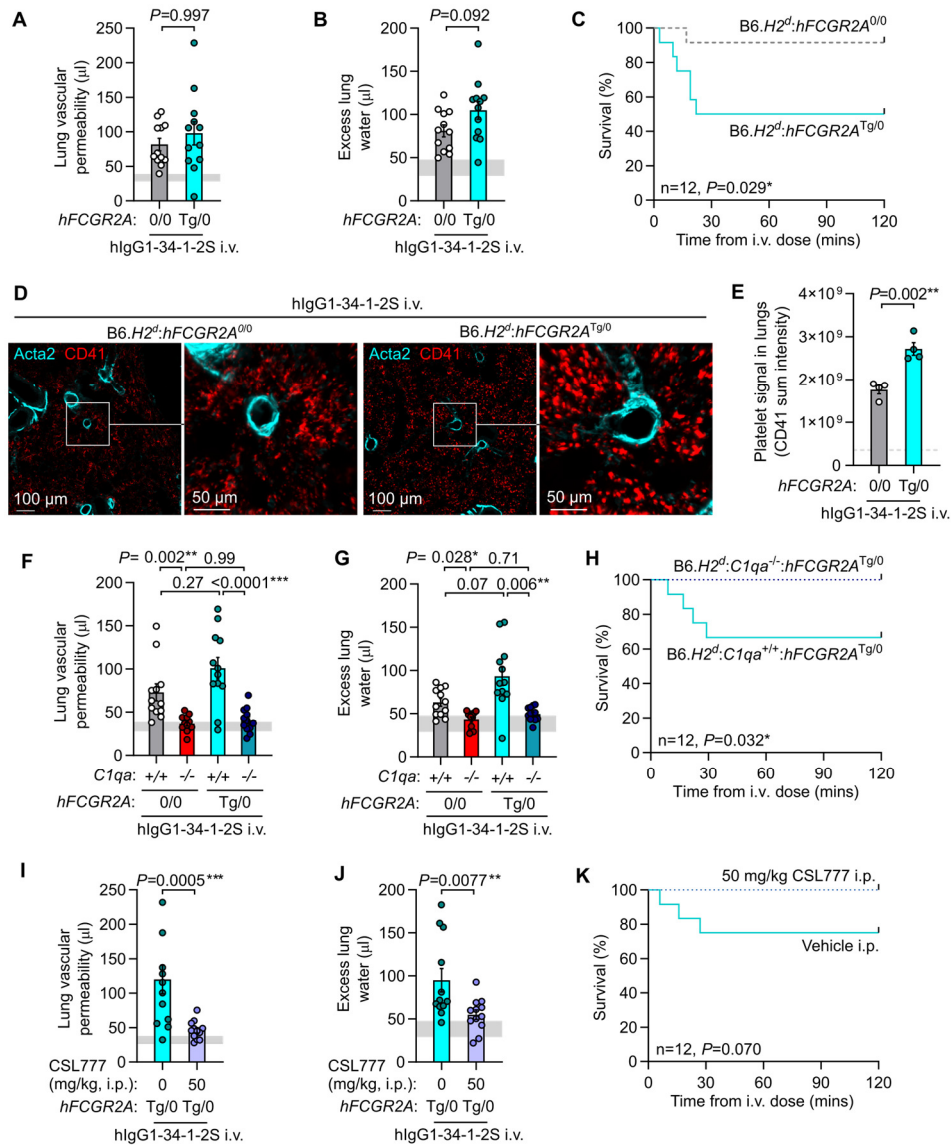
Graphs show means ± standard errors with horizontal line representing standard deviations from 'no injury' controls (from vehicle + isotype control group). Log$_{10}$-transformed data were analyzed using either (**C**, **D**) an ordinary one-way ANOVA with P-values from Dunnett's multiple comparisons test for difference relative to vehicle + 34-1-2S group, or (**E**, **F**) two-tailed unpaired t-test, with group n=10.

542

Fig. 6. Acute lung injury is complement-dependent in a model incorporating human FCGR2A-mediated pathology.

A. Lung vascular permeability, **B**. excess lung water and **C**. survival readouts from LPS-primed B6.$H2^d$:$hFCGR2a^{Tg/0}$ mice and B6.$H2^d$ littermate controls given i.v. hIgG1-34-1-2S at 1 mg/kg.

D. Immunofluorescence imaging of platelet sequestration (CD41, red, with Acta2 in cyan) in lungs from B6.$H2^d$:$hFCGR2a^{Tg/0}$ mice and littermates without hFCGR2A fixed at 20 minutes after hIgG1-34-1-2S injections, quantified in **E**.

F. Lung vascular permeability, **G**. excess lung water and **H**. survival readouts from LPS-primed B6.$H2^d$:$C1qa^{+/+}$ and B6.$H2^d$:$C1qa^{-/-}$ mice, as well as littermates of each genotype expressing hFCGR2A, given i.v. hIgG1-34-1-2S at 1 mg/kg.

I. Lung vascular permeability, **J**. excess lung water and **K**. survival readouts from LPS-primed B6.$H2^d$:$hFCGR2a^{Tg/0}$ mice given either vehicle or 50 mg/kg CSL777 i.p. before i.v. hIgG1-34-1-2S at 1 mg/kg.

A, B, E, F, G, I & J show means ± standard errors with horizontal gray lines showing means or standard deviations of values from 'no injury' controls (B6.$H2^d$ mice given LPS i.p. + hIgG1 isotype control i.v.) and were $\log_{10}$-transformed prior to analysis. P-values are from: (**A, B, I, J**) unpaired, two tailed t-tests; (**F, G**) two-way ANOVA with Šídák's multiple comparisons test; or (**C, H, K**) log-rank test, with group n=4 (**E**) or 12 (other graphs).